Met. Mater. Int., Vol. 20, No. 5 (2014), pp. 975~981
doi: 10.1007/s12540-014-5024-8

One-Step Preparation of Reduced Graphene Oxide/Carbon Nanotube Hybrid Thin Film by Electrostatic Spray Deposition for Supercapacitor Applications

Hee-Chang Youn[1], Seong-Min Bak[1], Sang-Hoon Park[1], Seung-Beom Yoon[1], Kwang Chul Roh[2,*], and Kwang-Bum Kim[1,*]

[1]Yonsei University, Department of Materials Science and Engineering, 134 Shinchon-dong, Seodaemoon-gu, Seoul 120-749, Korea
[2]Korea Institute of Ceramic Engineering & Technology, Energy Efficient Materials Team, Energy & Environmental Division, 233-5 Gasan-dong, Guemcheon-gu, Seoul 153-801, Korea

(received date: 5 November 2013 / accepted date: 30 December 2013)

In this paper, we describe a binder-free reduced graphene oxide/carbon nanotube hybrid thin film electrode prepared using a one-step electrostatic spray deposition method. Though we introduce a novel method, we suspect that the greater potential impact is more related to the fact that this technique is able to accomplish producing an electrode with a single process and allows a degree of control over the film properties not yet found in other fabrication methods that require multiple steps (that include post processing). In order to investigate the effect of carbon nanotube as a nano-spacer on the electrochemical properties of the reduced graphene oxide/carbon nanotube hybrid thin film electrodes, the various content of carbon nanotube was incorporated between the 2 dimensional layered reduced graphene oxide sheets to prevent restacking among reduced graphene oxide sheets and their electrochemical properties were systemically investigated using cyclic voltammetry, galvanostatic charge/discharge test and electrochemical impedance spectroscopy. The hybrid thin film electrode delivered a higher reversible specific capacitance of 187 $F \cdot g^{-1}$ at 0.5 $A \cdot g^{-1}$ and showed a better rate capability by maintaining 73% of the specific capacitance at 16 $A \cdot g^{-1}$ (vs. 0.5 $A \cdot g^{-1}$), which exhibit remarkable electrochemical performances than a RGO thin film electrodes for supercapacitor applications.

Keywords: capacitors, energy storage materials, nanostrctured materials, depositions, thin films

1. INTRODUCTION

Graphene has a two-dimensional honeycomb structure consisting of a single layer of carbon atoms with a sp^2-bonding configuration and has recently attracted significant attention owing to its unique properties, which include an exceptionally high specific surface area and high electrical and thermal conductivities as well as mechanical and chemical stability [1-4]. Reduced graphene oxide (RGO) has most commonly been prepared by the chemical reduction and thermal exfoliation of graphite oxides, which themselves are usually produced by the oxidation of pristine graphite [5,6]. However, RGO sheets prepared in this manner exhibit an extreme tendency to agglomerate or restack. This leads to a surface that is electrochemically less effective, low electrical conductivity, and an interlayer spacing that hinders access to electrolyte ions, thus limiting the use of the sheets in supercapacitor applications [7,8] Introducing carbonaceous materials such as carbon nanotube (CNT) between the RGO sheets is a viable strategy for preventing the sheets from agglomerating [9,10]. There have already been a few efforts to fabricate solution-processable RGO sheets, which are then treated by solution reduction and refunctionalization in order to obtain a stable colloidal suspension in order to form RGO-based film electrodes, including RGO/CNT hybrid ones. These efforts have utilized methods such as filtration, solution casting, electrophoretic deposition, spin coating, and layer-by-layer electrostatic self-assembly [8,11-16] However, most of these methods for fabricating hybrid electrodes require separate development before they can be used to form hybrid materials, and they also require methods for removing the dispersive media such as oxygen functional groups or organic surfactants attached to the graphene oxide and CNT surfaces.

Herein, we report the fabrication of a RGO/CNT hybrid thin film in a one-step process that involves electrostatic spray deposition (ESD). This technique allows the graphene oxide and acid-treated CNT (a-CNT) surfaces to be defunctional-

*Corresponding author: kbkim@yonsei.ac.kr, rkc@kicet.re.kr

ized by thermal decomposition (thus precluding the need for a post-fabrication treatment), and the fabrication of a binder-free hybrid electrode on a metal-coated substrate from a homogeneous mixed colloidal suspension consisting of graphene oxide and a-CNT can be performed simultaneously. The hybrid thin film produced using this technique exhibited uniform surface morphologies and good adhesion on the substrate. In addition, the mass, thickness, and operating temperature of the electrodes could also be controlled [17]. In order to electrochemically investigate the effects of incorporating CNT between the RGO sheets, we compared the performance of a RGO/CNT hybrid thin film electrode against that of a RGO thin film electrode prepared in a similar fashion.

2. EXPERIMENTAL PROCEDURE

2.1. Synthesis of graphite oxide

First, 14 g of potassium permanganate ($KMnO_4$, 99%, Sigma-Aldrich) was added into a mixture comprising 4 g of pristine graphite flakes (nominal particle size: 45 μm, Sigma-Aldrich) and 100 mL of concentrated sulfuric acid (H_2SO_4, 95%, Samchun Chemical Co., Ltd.). The oxidation treatment of the mixture was allowed to proceed at 35 °C for 5 h. Then, 150 mL of distilled water and 50 mL of hydrogen peroxide (H_2O_2, 35%, Junsei Chemical Co., Ltd.) were added drop by drop into the mixture until gas could no longer be seen evolving. Upon the addition of H_2O_2, the yellow-brownish oxidation product of graphite was observed in the form of a colloidal suspension. This yellow-brownish colloidal suspension was then repeatedly washed and centrifuged with 0.3 M hydrochloric acid (HCl, 35-37%, Samchun Chemical Co., Ltd.) and distilled water. Finally, the resulting yellow-brownish powder was freeze-dried and collected.

2.2. Synthesis of acid-treated carbon nanotube (a-CNT)

Pristine CNT (CM95, Hanwha Nanotech Corp.) cannot be dispersed in polar solvents. Hence, an oxidation treatment was performed using the Hummers method to introduce oxygen functional groups on the hydrophobic CNT surfaces in order to form a stable colloidal suspension of the CNT in polar solvents.

2.3. Fabrication of the RGO/CNT hybrid thin film electrode by ESD

The fabrication of the RGO/CNT hybrid thin film electrode was performed in two steps. The first step was the preparation of a uniformly dispersed colloidal suspension of graphite oxide and the a-CNT with mass ratios of 90:10, 70:30, 50:50, 30:70, 10:90 in a mixture of water and ethanol by ultra-sonication for 1 h. This colloidal suspension could be maintained for several weeks without any sedimentation. The second step was ESD of the colloidal suspension onto a platinum-coated silicon wafer substrate to prepare the RGO/CNT hybrid thin film electrode. The platinum-coated silicon wafer substrate, which served as a current collector, was heated to a suitably high temperature (300 °C). Heating the substrate helped promote the defunctionalization of the graphene oxide and a-CNT during the fabrication of the RGO/CNT hybrid thin film electrode. The resulting precursor suspension was pumped at a rate of 8-15 $mL \cdot h^{-1}$ while the DC potential difference between the nozzle of the syringe and the substrate was set at 10-15 kV. In this way, RGO/CNT hybrid thin film electrodes were fabricated without any post-fabrication treatment and could be used as working electrodes for further analysis. It should be noted that the mass ratios of RGO and CNT in the hybrid electrodes were determined by considering the C/O ratios of the RGO/CNT hybrid, as-prepared graphene oxide, and a-CNT. The mass ratios of the RGO and CNT in the hybrid electrodes were calculated to be 88:12, 65:35, 45:55, 26:74 and 9:91, respectively.

2.4. Characterization of the RGO/CNT hybrid thin film electrode

The structural characteristics of graphite oxide, the a-CNT, and the RGO/CNT hybrid thin film electrode were determined by X-ray diffraction (XRD) analyses and X-ray photoelectron spectroscopy (XPS). Fourier transform infrared spectroscopy (FTIR) was performed on the graphite oxide and a-CNT powders. The RGO/CNT hybrid materials were peeled from the platinum-coated silicon wafer substrate for the FTIR-based analysis. The XRD (DMAX-2200, Rigaku) patterns were recorded over 2θ of 5-30° using Cu Kα radiation (λ = 1.54056 Å). The XPS-based measurements were performed using an ESCA 2000 spectrometer (VG Microtech) with monochromated Al Kα radiation ($h\nu$ = 1486.6 eV). The FTIR spectra were obtained over wavelengths of 4000-450 cm^{-1} at a spectral resolution of 4 cm^{-1} using KBr pellets at room temperature with a Perkin Elmer 1710 spectrophotometer. The microstructures of the RGO/CNT hybrid and RGO thin film electrodes were examined using a scanning electron microscope (SEM) (S-4300E, Hitachi). The electrochemical properties of the two thin film electrodes were investigated at room temperature using a three-electrode cell with a platinum plate as the counter electrode and a saturated calomel electrode (SCE) as the reference electrode. Cyclic voltammetry (CV) and galvanostatic charge/discharge analyses were performed using a potentiostat/galvanostat (VMP3, Princeton Applied Research) with a 1 M aqueous solution of H_2SO_4 as the electrolyte. The analyses were performed over the potential window of 0-1 V (vs. SCE (V_{SCE})) at scan rates of 5-200 $mV \cdot s^{-1}$ and current densities of 0.5-16 $A \cdot g^{-1}$. In addition, electrochemical impedance spectroscopy (EIS)-based measurements were performed using an impedance analyzer (Solartron 1260A, Impedance/Gain-Phase Analyzer) at a DC bias voltage of 0.2 V_{SCE} over AC frequencies ranging from 200 kHz to 10 MHz and an AC amplitude of 5 mV. A 1.0 M aqueous solution of H_2SO_4 was used as the electrolyte.

3. RESULTS AND DISCUSSION

Scheme 1 illustrates the proposed method for the ESD synthesis of a RGO/CNT hybrid thin film electrode. A stable colloidal suspension consisting of graphene oxide and a-CNT was prepared by ultrasonically dispersing a mixture of graphene oxide and a-CNT in a mixed solution of water and ethanol with a volume ratio of 1:1. Since the functional groups in the polar solvent were ionized, a stable colloidal suspension could be formed readily because of the electrostatic repulsion between the negatively charged surfaces of the graphene oxide and a-CNT [8]. The suspension was then sprayed onto a platinum-coated silicon wafer substrate, which was heated to a temperature high enough (300 °C) to promote the defunctionalization of the graphene oxide and a-CNT by the thermal decomposition of their functional groups. Thus, both the reduction of the graphene oxide and a-CNT and the formation of a hybrid thin film electrode could be achieved in a single step.

The microstructure of the thus-fabricated RGO based-electrode prepared by using ESD technique was investigated with an SEM. As can be seen clearly from the basal plane view SEM image in inset of Fig. 1(a), the RGO sheets and CNT were evenly dispersed, forming numerous pores in the hybrid thin film electrode. Furthermore, as can be seen from the cross-sectional view SEM image in Fig. 1(a), the RGO/CNT hybrid electrode had a layered structure with the CNT evenly sandwiched between the RGO sheets as spacers. The CNT incorporated between the RGO sheets promoted the formation of the porous structure in the hybrid thin film electrode. The microstructure of the RGO/CNT hybrid electrode was observably different from that of a RGO thin film electrode prepared in a similar fashion shown in Fig. 1(b). The slightly wrinkled and 2-dimensional homogeneous sheets without any pores, which seem to be compacted and stacked together firmly, are exhibit for RGO thin film electrode.

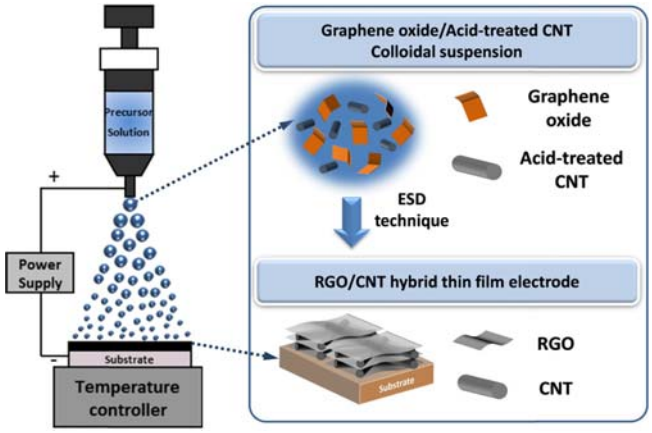

Scheme 1. Schematic illustration of the fabrication of a reduced graphene oxide (RGO)/carbon nanotube (CNT) hybrid thin film electrode by electrostatic spray deposition (ESD).

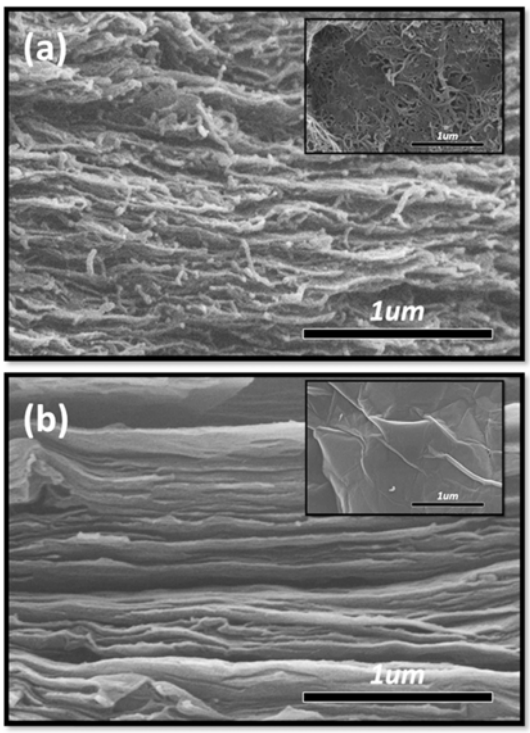

Fig. 1. SEM images of the RGO/CTN hybrid thin film; (a) cross-sectional view (Inset : basal plane view) and those of the RGO thin film electrode; (b) cross-sectional view (Inset : basal plane view).

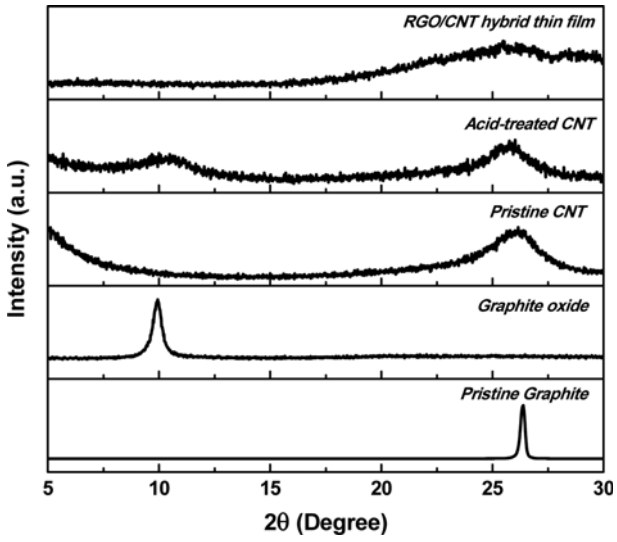

Fig. 2. (a) XRD patterns of the pristine graphite, graphite oxide, pristine CNT, acid-treated CNT and RGO/CNT hybrid thin film.

The XRD spectrum (Fig. 2) of the RGO/CNT hybrid thin film shows how its structure differed from those of graphite oxide and the a-CNT. In the XRD spectra of pristine graphite and CNT, the major diffraction peak at $2\theta = 26°$ indicates a highly oriented graphitic structure with an interlayer spacing of 0.34 nm. On the other hand, the major diffraction peak in the XRD spectrum of graphite oxide ($2\theta = 9.76°$) indicates an

increased interlayer spacing of the graphene layers of 0.91 nm, while those in the a-CNT spectra (2θ = 10.23°, d = 0.86 nm; 2θ = 26°, d = 0.34 nm) suggest that the CNT are multiwalled and that there exists an oxidized outer layer for d-spacing of 0.86 and non-oxidized inner layer for d-spacing of 0.34 nm, which are oriented along the (002) plane [18]. In the RGO/CNT hybrid thin film electrode XRD spectrum, there were no diffraction peaks around 2θ = 9.76° for graphite oxide and 2θ = 10.23° for a-CNT that could be attributed to an oxidized surface, and the peak at 2θ = 26° was ascribable to the inner (002) plane of the CNT. The post-ESD diffraction pattern of every entity was different from its pre-ESD diffraction pattern, owing to the defunctionalization of the graphene oxide and a-CNT during the deposition process. This was also the case for their FTIR spectra of the graphite oxide, a-CNT, and RGO/CNT hybrid thin film electrode (Fig. 3). The FTIR peaks for oxygen functional groups at 1726 cm^{-1} (C=O stretching vibration for the carbonyl and carboxylic groups), 1226 cm^{-1} (C-OH stretching vibration from the hydroxyl groups), and 1052 cm^{-1} (C-O stretching vibration) are clearly observed in the spectra of graphite oxide and a-CNT. Such functional groups are favorable to the formation of a stable colloidal suspension of graphene oxide and a-CNT, because of the highly negative surface charge of the as-prepared graphene oxide and a-CNT from the ionization of oxygen functional groups, and the electrostatic repulsion force among the graphene oxide sheets and a-CNT in the polar solvents. Those peaks for oxygen functional groups were significantly reduced after the ESD process during the preparation of the RGO/CNT hybrid thin film electrode, which is due to the defunctionalization of the graphene oxide and a-CNT during the deposition process.

XPS was used to quantitatively investigate the changes in the atomic concentrations of the functional groups after the ESD process (Fig. 4). The peak intensities for carbon atom

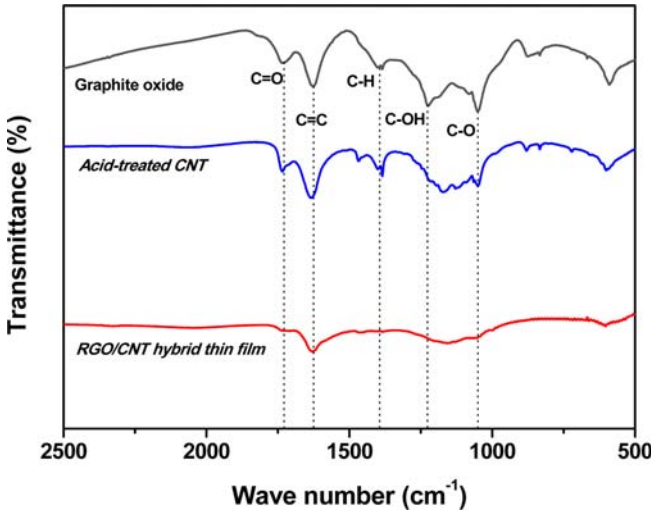

Fig. 3. FT-IR spectra of the RGO/CNT hybrid thin film, acid-treated CNT, and graphite oxide.

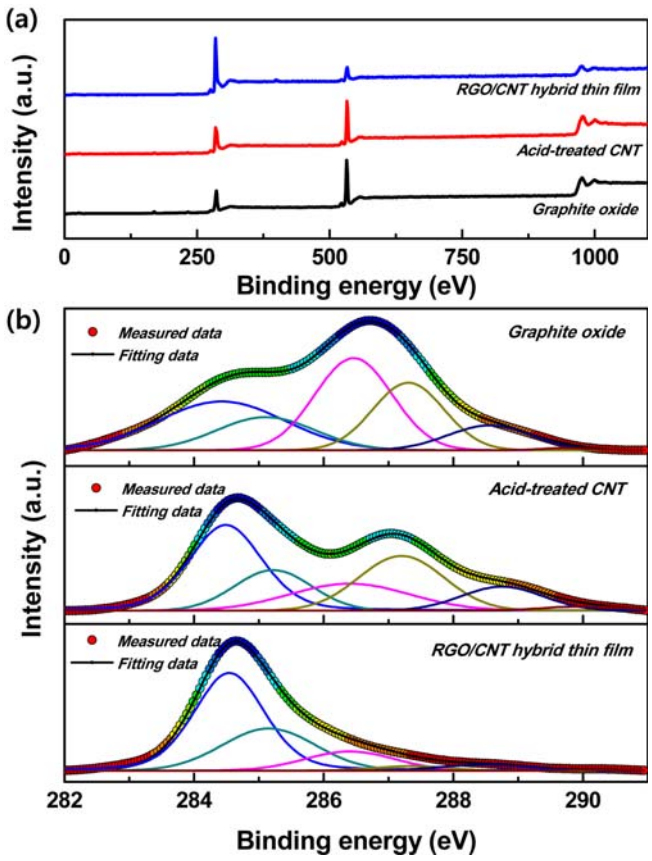

Fig. 4. (a) Full-scale XPS spectra of the RGO/CNT hybrid electrode, acid-treated CNT, and graphite oxide. (b) Deconvolution of the C1s XPS spectra of the RGO/CNT hybrid thin film, acid-treated CNT, graphite oxide.

(C1s, 285 eV) and oxygen atom (O1s, 530 eV) are obviously reversed after the ESD process for preparation of RGO/CNT hybrid thin film in Fig. 4(a). This is due to the reduction of the graphite oxide and a-CNT. The deconvolution of the C1s spectra in Fig. 4(b) yields five peaks with different binding energies representing the following carbon bonds: C=C (sp^2 at 284.5 eV), C-C (sp^3 at 285.2eV), C-O (at 286.4 eV), C=O (at 287.3 eV), and C(O)O (at 288.5 eV) [19] and the atomic concentration of those bonds in graphite oxide, a-CNT, and RGO/CNT hybrid thin film was exhibited in Table 1, which are calculated by the deconvolution of C1s XPS spectra of the various entities. The deconvolution data for graphite oxide and the a-CNT in Fig 4(b) show that the peaks for the C-O, C=O, and C(O)O bonds were of high intensity. This signifies that functional groups were strongly attached to the graphite oxide and a-CNT surfaces by the oxidation treatment. After the ESD process, the intensities of these three peaks were significantly reduced owing to the defunctionalization of the graphite oxide and a-CNT. The atomic concentrations of sp^2 and sp^3 bonds (C=C : 54.2 at% and C-C : 27.5 at%, respectively) in the hybrid thin film electrode were higher than

Table 1. Atomic concentration (at. %) of different types of carbon bonds in the graphite oxide, acid-treated CNT, and RGO/CNT hybrid thin film

	C=C (sp^2)	C-C (sp^3)	C-O	C=O	C(O)O	pi-pi*
Graphite oxide	26.3	13.8	30.2	20.4	8.8	0.4
Acid-treated CNT	34.3	15.4	15.9	23.0	9.6	1.7
RGO/CNT hybrid thin film	54.2	27.5	12.0	2.3	3.7	0.3

The values shown were calculated by the deconvolution of C1s XPS spectra of the various entities.

those in graphite oxide (C=C: 26.3 at% and C-C: 13.8 at%) and the a-CNT (C=C: 34.3 at% and C-C: 15.4 at%). On the other hand, the atomic concentrations of the C-O, C=O, and C(O)O groups in the hybrid thin film were considerably lower (Table 1); this is also proof of the defunctionalization of the graphite oxide and a-CNT.

CV, galvanostatic charge and discharge tests, and EIS were used to investigate the electrochemical properties of the RGO thin film electrode and RGO/CNT hybrid thin film electrode. Fig. 5(a) exhibits the CV curves of the RGO/CNT hybrid thin film electrode for scan rates ranging from 5 to 200 $mV \cdot s^{-1}$. The curves are quasi-rectangular, which is indicative of the capacitive behavior of the electrode and the coexistence of an electric double layer capacitance and a pseudocapacitance. The pseudocapacitance derives from the reversible redox reaction of the residual functional groups superimposed at ~0.4 V_{SCE} for the anodic scan and at ~0.35 V_{SCE} for the cathodic scan [20]. Furthermore, the electrode's high rate capability is demonstrated by the fact that the quasi-rectangular shape is maintained for scan rates of up to 200 $mV \cdot s^{-1}$. For the purpose of comparison, the RGO thin film electrode was also electrochemically characterized in a similar fashion shown in Fig. 5(b). The CV curves for RGO thin film electrode are also quasi-rectangular. However these had an extremely diminished current response and exhibited increased curve distortion at higher scan rates. Thus, it can be inferred that the RGO/CNT

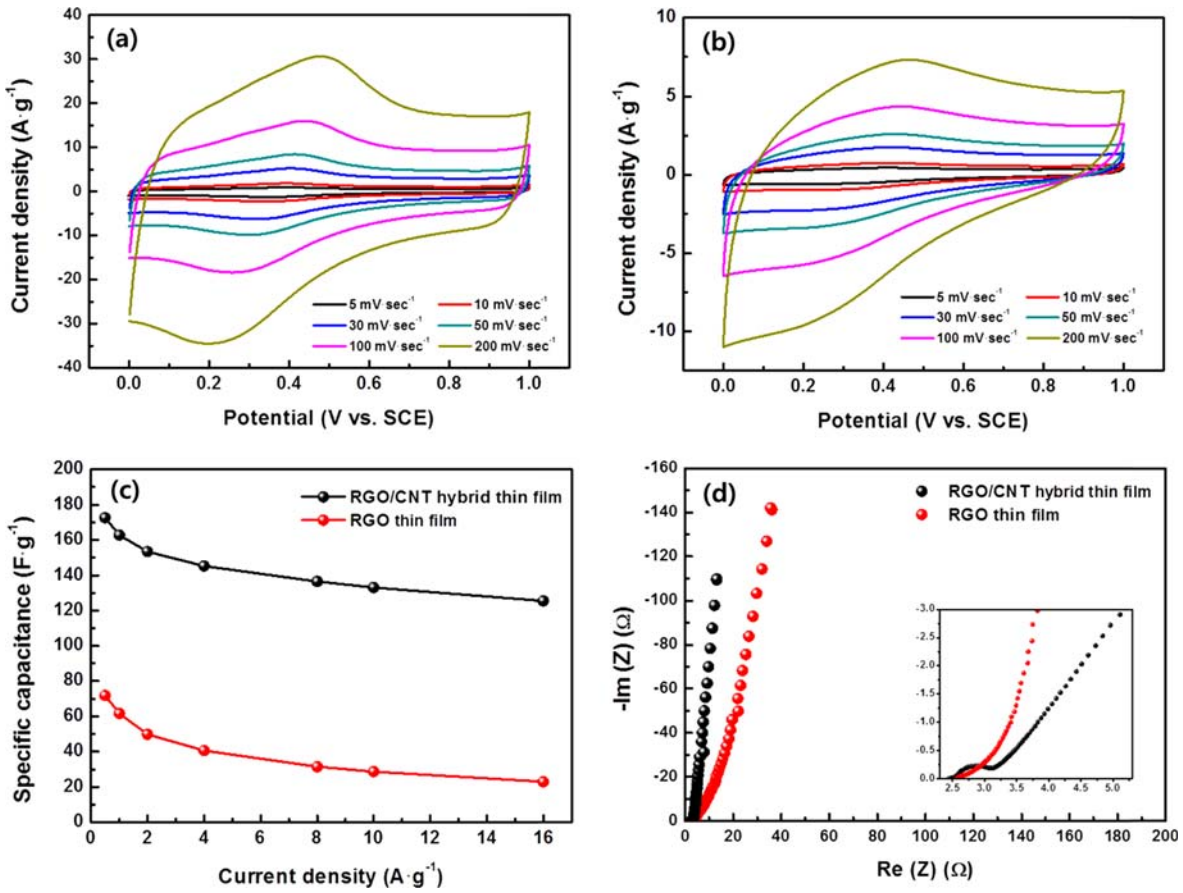

Fig. 5. Cyclic voltammograms of (a) the RGO thin film electrode and (b) the RGO/CNT hybrid electrode at various scan rates (5-200 $mV \cdot sec^{-1}$). (c)The rate capabilities of the RGO thin film and RGO/CNT hybrid thin film electrode. (d) Nyquist plot of the RGO thin film and RGO/CNT hybrid thin film electrodes. The gravimetric capacitances were calculated using the results of galvanostatic charge/discharge tests performed at current densities ranging from 0.5 to 16 $A \cdot g^{-1}$.

hybrid electrode greatly outperforms the plain RGO electrode at higher scan rates.

Figure 5(c) shows the specific capacitance of the RGO/CNT hybrid electrode for current densities ranging from 0.5 to 16 $A \cdot g^{-1}$. Its specific capacitance was calculated to be 187 $F \cdot g^{-1}$ at 0.5 $A \cdot g^{-1}$, which is significantly higher than the specific capacitance of the RGO electrode (72 $F \cdot g^{-1}$ at 0.5 $A \cdot g^{-1}$) and indicates that the surface area of the former was higher and electrochemically more effective. Furthermore, the fact that the specific capacitance of the RGO/CNT hybrid electrode decreased by 73% when the current density was increased from 0.5 to 16 $A \cdot g^{-1}$ highlights its excellent rate capability. Since the rate capability of a supercapacitor is highly dependent on the ease with which the electrolyte ions can access the reaction sites through the electrode (i.e., on the porous structure of the electrode), it can be inferred that the CNT spacers in the hybrid electrode serve to facilitate the formation of a porous structure and hence improve the ion accessibility of the reaction sites.

Figure 5(d) shows the Nyquist plots for the RGO/CNT hybrid thin film and RGO thin film electrodes obtained by EIS. In the low-frequency region, the imaginary part for the hybrid electrode is almost a vertical line, indicating that the electrode exhibits better capacitive behavior than the RGO thin film electrode. The radius of the semicircle for the hybrid electrode decreases in the high-frequency region, which reflects a lower polarization impedance compared to that of the RGO thin film electrode [21,22]. This can be attributed to the porous structure of the hybrid thin film electrode, which allows the electrolyte ions to be transferred into the electrode more readily.

Figure 6 shows the specific capacitance and the high rate capability of the RGO/CNT hybrid thin film electrodes as a function of CNT content, pure RGO and pure CNT thin film electrodes. In this study, the ratio of specific capacitances at 0.5 and 16 $A \cdot g^{-1}$ was taken as a measure of the high rate capability of each electrode. The specific capacitance of the RGO/CNT hybrid thin film electrode sharply increased from 72 to 201 $F \cdot g^{-1}$ with the addition of 12 wt% CNTs. With further incorporation of the CNTs, the specific capacitance of the RGO/CNT hybrid thin film electrodes decreased linearly as a function of the CNT content, and reached a specific capacitance of 110 $F \cdot g^{-1}$ for the pure CNT electrode. It is noteworthy that the CNT acts as the spacer for preventing the agglomeration and/or restacking of RGO sheets as well as an electro-active material to provide an additional specific capacitance. The linear change in the specific capacitance of the RGO/CNT hybrid thin film electrodes indicates that the specific capacitance of the hybrid electrode could be calculated on the assumption of the rule of mixtures of the specific capacitances of the 88:12 wt% RGO/CNT hybrid and pure CNT thin film electrodes. It suggests that the effective surface area of RGO sheets in the hybrid electrodes is relatively constant, even when the CNT content in the RGO/CNT hybrid thin film electrodes is increased above 12 wt%. Comparison of the specific capacitances of the pure RGO electrode and the imaginary pure RGO electrode indicates the important role of CNTs as a spacer to the improvement of the effective surface area of RGO sheets, and the specific capacitance of hybrid electrodes.

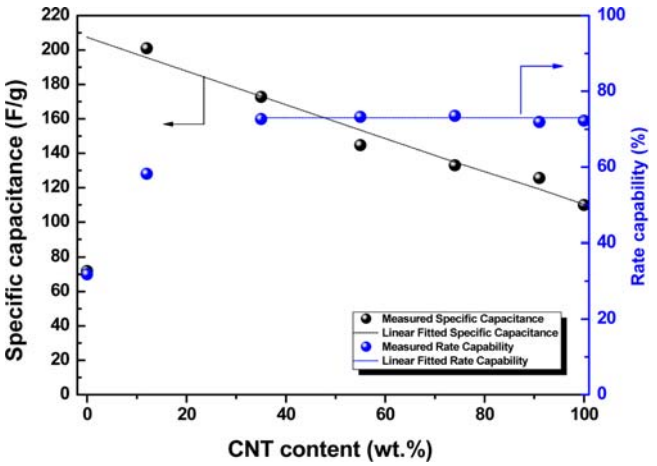

Fig. 6. Specific capacitance and high rate capability of the RGO/CNT hybrid electrodes as a function of CNT content, pure RGO and pure CNT electrodes.

Figure 6 also shows the rate capability of RGO hybrid electrodes as a function of CNT content; the rate capability increases with the incorporation of CNTs up to 35 wt%, and stays constant with the further addition of CNTs. Since the rate capability of the RGO/CNT hybrid thin film electrodes is highly dependent on ion accessibility to reaction sites through a porous electrode structure, as well as on electric conductivity, it can be inferred that the CNTs in the hybrid electrode could facilitate the formation of porous electrode structure, and thereby the ion accessibility to reaction sites. However, excessive incorporation of CNTs did not seem to further improve ion accessibility.

4. CONCLUSIONS

In summary, a RGO/CNT hybrid thin film electrode was successfully prepared using electrostatic spray deposition. This is the first report of the preparation of an RGO-based electrode in this manner. Using this technique, it is possible to defunctionalize graphite oxide and a-CNT by thermal decomposition and fabricate a binder-free hybrid electrode simultaneously. The RGO/CNT hybrid electrode exhibited better electrochemical performance than a plain RGO electrode in terms of their specific capacitances and rate capabilities. It was found that the incorporation of the CNT in the hybrid electrode not only increases the electrochemically effective surface area but also prevents the restacking or agglomeration of the RGO sheets, promotes the formation of a porous structure with an interlayer spacing large enough to

positively affect electrolyte ion accessibility, and enhances the electrical conductivity of the electrode.

ACKNOWLEDGMENTS

This work was supported by the energy efficiency and resources of the Korea Institute of Energy Technology Evaluation and Planning (KETEP) grant funded by the Ministry of Knowledge Economy, Korean government (No: 20122010100140) and (No: 2010T100200232).

REFERENCES

1. K. S. Novoselov, A. K. Geim, S. V. Morozov, D. Jiang, Y. Zhang, S. V. Dubonos, I. V. Grigorieva, and A. A. Firsov, *Science* **306**, 666 (2004).
2. M. D. Stoller, S. Park, Y. Zhu, J. An, and R. S. Ruoff, *Nano Lett.* **8**, 3498 (2008).
3. L. Rodriguez-Perez, M. A. A. Herranz, and N. Martin, *Chem. Comm.* **49**, 3721 (2013).
4. J. H. Lee, D. H. Cho, S. C. Kim, S. G. Baek, J. G. Lee, J. M. Kang, J.-B. Choi, C. S. Seok, M. K. Kim, J. C. Koo, and B. S. Lim, *Korean J. Met. Mater.* **50**, 206 (2012).
5. M. J. McAllister, J.-L. Li, D. H. Adamson, H. C. Schniepp, A. A. Abdala, J. Liu, M. Herrera-Alonso, D. L. Milius, R. Car, R. K. Prud'homme, and I. A. Aksay, *Chem. Mater.* **19**, 4396 (2007).
6. S. Stankovich, D. A. Dikin, R. D. Piner, K. A. Kohlhaas, A. Kleinhammes, Y. Jia, Y. Wu, S. T. Nguyen, and R. S. Ruoff, *Carbon* **45**, 1558 (2007).
7. Y. Si and E. T. Samulski, *Nano Lett.* **8**, 1679 (2008).
8. D. Li, M. B. Muller, S. Gilje, R. B. Kaner, and G. G. Wallace, *Nat. Nanotech.* **3**, 101 (2008).
9. J. Yan, T. Wei, B. Shao, F. Ma, Z. Fan, M. Zhang, C. Zheng, Y. Shang, W. Qian, and F. Wei, *Carbon* **48**, 1731 (2010).
10. Z. Lei, N. Christov, and X. S. Zhao, *Energy Environ. Sci.* **4**, 1866 (2011).
11. Y. Xu, H. Bai, G. Lu, C. Li, and G. Shi, *J. Am. Chem. Soc.* **130**, 5856 (2008).
12. D. Cai, M. Song, and C. Xu, *Adv. Mater.* **20**, 1706 (2008).
13. Z.-S. Wu, S. Pei, W. Ren, D. Tang, L. Gao, B. Liu, F. Li, C. Liu, and H.-M. Cheng, *Adv. Mater.* **21**, 1756 (2009).
14. X. Li, G. Zhang, X. Bai, X. Sun, X. Wang, E. Wang, and H. Dai, *Nat. Nanotech.* **3**, 538 (2008).
15. J. Liu, J. Tang, and J. J. Gooding, *J. Mater. Chem.* **22**, 12435 (2012).
16. J. H. Kang, J. M. Choi, J.Y. Hyeon, and J. H. Sok, *Korean J. Met. Mater.* **52**, 55 (2014).
17. J. H. Kim, K.W. Nam, S. B. Ma, and K.-B. Kim, *Carbon* **44**, 1963 (2006).
18. D. V. Kosynkin, A. L. Higginbotham, A. Sinitskii, J. R. Lomeda, A. Dimiev, B. K. Price, and J. M. Tour, *Nature* **458**, 872 (2009).
19. D. R. Dreyer, S. Park, C. W. Bielawski, and R. S. Ruoff, *Chem. Soc. Rev.* **39**, 228 (2010).
20. Z. Lin, Y. Liu, Y. Yao, O. J. Hildreth, Z. Li, K. Moon, and C.-P. Wong, *J/ Phys. Chem. C* **115**, 7120 (2011).
21. X. Du, P. Guo, H. Song, and X. Chen, *Electrochim. Acta* **55**, 4812 (2010).
22. J. Gamby, P. L. Taberna, P. Simon, J. F. Fauvarque, and M. Chesneau, *J Power Sources* **101**, 109 (2001).